



## Toward an on-line characterization of kaolin calcination process using short-wave infrared spectroscopy

A. Guatame-García <sup>a</sup>, M. Buxton<sup>a</sup>, F. Deon<sup>a</sup>, C. Lievens<sup>b</sup>, and C. Hecker <sup>b</sup>

<sup>a</sup>Resource Engineering, Faculty of Civil Engineering and Geosciences, Delft University of Technology, Delft, The Netherlands; <sup>b</sup>Department of Earth Systems Analysis, Faculty of Geo-Information Science and Earth Observation (ITC), University of Twente, Enschede, The Netherlands

### ABSTRACT

In the production of calcined kaolin, the on-line monitoring of the calcination reaction is becoming more relevant for the generation of optimal products. In this context, this study aimed to assess the suitability of using infrared (IR) spectroscopy as a potential technique for the on-line characterization of the calcination of kaolin. The transformation of kaolin samples calcined at different temperatures were characterized in the short-wave (SWIR) spectra using the kaolinite crystallinity (Kx) index and the depth of the water spectral feature (1900D). A high correlation between the standard operational procedure for the quality control of calcined kaolin and the Kx index was observed ( $r = -0.89$ ), as well as with the 1900D parameter ( $r = -0.96$ ). This study offers a new conceptual approach to the use of SWIR spectroscopy for the characterization the calcination of kaolin, withdrawing the need of using extensive laboratory techniques.

### KEYWORDS

Kaolinite; metakaolinite;  $\gamma$ -alumina; calcined kaolin; SWIR–MWIR–LWIR spectroscopy; process control

## 1 Introduction

For industrial applications, natural kaolin clay is heated to temperatures above 900°C. The purpose of this thermal treatment, also known as calcination, is to modify the chemical and physical properties and to enhance the value of the raw material. During the calcination, kaolinite [ $\text{Al}_2\text{Si}_2\text{O}_5(\text{OH})_4$ ], which is the main constituent in kaolin, is transformed first into metakaolinite [ $\text{Al}_2\text{Si}_2\text{O}_7$ ] and further into mullite [ $\text{Al}_2\text{SiO}_5$ ]. The industrial interest on calcined kaolin depends on the chemical and physical properties of the intermediate phases produced at various calcination stages. For example, the highly disordered and reactive metakaolinite is used as a pozzolanic additive in the cement industry. For other uses, such as in the pharmaceutical industry, the calcination time is increased to reduce the metakaolinite chemical reactivity and enhance the whiteness, yet keeping low abrasiveness (Thomas et al. 2009). The high-temperature mullite phase is whiter than metakaolinite, but highly abrasive, which is detrimental for the targeted markets. In order to ensure the production of calcined kaolin with optimum properties, the quality control strategies should involve techniques that enable a quick turn-around for timely operational feedback. It is then required that such techniques can be used in an on-line production environment and generate (near) real-time data. However, the study of calcined kaolin in the industry has focused mostly on product development rather than in the monitoring and control of the calcination process.

The standard operating procedure in the industry for the quality control of calcined kaolin products is the chemical

extraction of soluble  $\text{Al}_2\text{O}_3$ . This parameter is used to estimate the intermediate stages between the metakaolinite and mullite phases; however, the extraction of soluble  $\text{Al}_2\text{O}_3$  is a time-consuming laboratory-based technique, which is contrary to the necessities of a production environment. Other techniques, such as X-ray diffraction (XRD), struggle with the characterization of the metakaolinite and the subsequent intermediate stages, due to their amorphous structure, as was already remarked by Brindley and Nakahira (1959a) and Percival et al. (1974). For the consideration of an alternative characterization technique, the capability of detecting both, crystalline and amorphous phases, and the possibility of implementation in an on-line environment are mandatory requirements.

Regarding the first condition, infrared (IR) spectroscopy has been successfully used by multiple researchers to characterize the calcined kaolin reaction sequence (Miller 1961; Freund 1974; Percival et al. 1974; Frost and Vassallo 1996; Frost et al. 2002; Drits et al. 2016). Using laboratory-based instruments, which commonly cover the wavelength range between 2.5  $\mu\text{m}$  and 16.00  $\mu\text{m}$ , known as mid- and long-wave infrared ranges (MWIR and LWIR, respectively), different spectral bands have been assigned to detect the kaolinite–metakaolinite and metakaolinite–mullite transitions. Concerning the second condition, IR spectroscopy in the wavelength range between 1.00  $\mu\text{m}$  and 2.50  $\mu\text{m}$ , known as short-wave infrared or SWIR, has been used before in on-line applications in other mineral processing environments (Haavisto and Hytyniemi, 2011). In these ranges, IR spectroscopy has been proven a suitable on-line technique because of the lower costs of the optics of the instruments and their commercial availability. However, for the on-line

characterization of the calcined kaolin reaction, the conditions to extrapolate the laboratory observations to a suitable on-line set-up in the SWIR have not been yet explored.

To be able to develop an on-line analysis tool that provides information along entire kaolin calcination reaction, it is necessary to identify the spectral features in the SWIR range that describe the kaolinite–metakaolinite–mullite transition. This study explores different spectral parameters that can be related to such processes, and assesses the suitability of using SWIR spectroscopy as a proxy for the determination of the industrial standard, with the objective of contributing to the development of a monitoring and control strategy for the production of calcined kaolin. This paper first presents a brief review of the known IR spectral features that characterize the calcined kaolin reaction sequence. Then, samples of Cornish kaolin calcined at different temperatures are analyzed using laboratory and portable IR spectrometers in various spectral ranges. A special focus is given to the characterization of the mineral transitions in the MWIR and LWIR ranges to improve the interpretation of the SWIR spectra, especially for the calcination stages that involve indirect observations. The results of the SWIR analyses are further compared with the standard soluble  $\text{Al}_2\text{O}_3$  test, and the observations are discussed with a view toward their implications for the on-line characterization of the calcined kaolin reaction.

## 2 Infrared spectroscopy and the calcined kaolin reaction

Infrared spectroscopy has become a popular technique among geochemists and mineralogists since it is a relatively rapid, inexpensive, and requires little or no sample preparation. Infrared is used to determine the structure of the minerals, and to define algorithms for remote sensing and on-site applications. Depending on the application and instrumentation, the IR spectrum is measured in frequencies or wavelengths. For laboratory applications, frequencies are typically expressed in wavenumbers ( $\text{cm}^{-1}$ ), whereas for remote sensing, hand-held and on-line applications, it is common to use wavelength expressed in micrometers ( $\mu\text{m}$ ). Likewise, the definition of the spectral ranges depends upon the application field. Since the scope of this paper is toward an on-line implementation, the remote sensing, hand-held, and on-line convention is used. In this sense, the units are given in wavelengths, and the spectral ranges are defined as visible-near infrared (VNIR), SWIR, MWIR, and LWIR. Table 1 presents the wavelength and wavenumber equivalent for the main spectral ranges and absorption bands used here.

### 2.1 Calcined kaolin reaction

In the IR spectrum, the absorption features are a function of the wavelength and are related to the vibrations of molecular bonds in the minerals, thus giving information about their structure. In the study of the calcined kaolin reaction, IR spectroscopy is particularly useful since it detects the structural changes between the mineral transitions, including the amorphous phases. The thermal treatment of kaolin involves

**Table 1.** Equivalent wavelengths and wavenumbers of the main spectral absorption band and ranges used in this work (based on Gupta, 2003 and Hackwell et al., 1996).

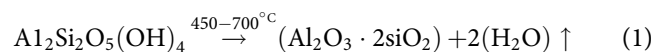
Spectral absorption band or range	Wavelength ( $\mu\text{m}$ )	Wavenumber ( $\text{cm}^{-1}$ )
VNIR range	0.35–1.00	28,571–10,000
SWIR range	1.00–2.50	10,000–4000
MWIR range	2.50–7.00	4000–1429
LWIR range	7.00–16.00	1429–625
Si–O (fundamental)	8.69–10.00, 11.10	1150–1000, 901
Al–O (fundamental)	12.39, 12.59, 13.29, 13.51	807, 794, 752, 740
Al–OH (fundamental)	10.66 and 10.94	938 and 914
Outer OH (fundamental)	2.70–2.77	3700–3600
Molecular $\text{H}_2\text{O}$ (fundamental)	2.74 and 6.13	3652 and 1630
Outer OH (overtone)	1.41	7092
OH and Al–OH (combination tone)	2.16 and 2.21	4629 and 4524
Molecular $\text{H}_2\text{O}$ (combination tone)	1.38 and 1.45, 1.88–1.90	7246 and 6896, 5319–5263

LWIR, long-wave infrared; MWIR, mid-wave infrared; SWIR, short-wave infrared; VNIR, visible-near infrared.

dehydration, dehydroxylation, and recrystallization (Heller-Kallai, 2013). Structural changes occur only in the last two phases, presented here as the low- and high-temperature calcination stages. In the low-temperature phase, kaolinite transforms into metakaolinite (Brindley and Nakahira, 1959b); in the high-temperature phase, metakaolinite recrystallizes to mullite (Brindley and Nakahira 1959c). The MWIR and LWIR ranges contain the fundamental vibrations that describe minerals thoroughly, whereas the VNIR and SWIR ranges contain overtones or combinations of the vibrations than contain OH-bonds. Traditionally, IR studies have focused on the MWIR and LWIR ranges to characterize the kaolinite–metakaolinite dehydroxylation process (Miller 1961; Percival et al. 1974; Frost and Vassallo 1996; Drits et al. 2016), and the re-crystallization from metakaolinite to mullite (Percival et al. 1974; Ptáček et al. 2011).

### Kaolinite–metakaolinite transition

In the low-temperature domain of the calcination reaction (500–800°C), the transformation of kaolinite into metakaolinite is characterized by the removal of the chemically bonded water and the breakdown of the hydroxyl bonds; metakaolinite contains a small proportion of residual hydroxyl groups, and after prolonged heating it releases water (Drits and Derkowski 2015). Consequently, the kaolinite–metakaolinite transformation occurs according to the reaction:



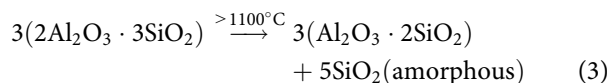
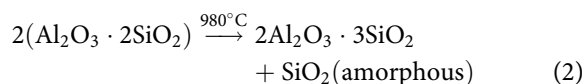
According to Murray and Lyons (1959), the rate of this transformation depends on the crystallinity of the primary kaolinite. Frost et al. (2002) Drits et al. (2016), and Percival et al. (1974) summarized the diagnostic spectral absorption bands of the kaolinite–metakaolinite transition (Figure 1). The aluminosilicate framework presents multiple absorptions related to Si–O bonds between 8.69  $\mu\text{m}$  and 10.00  $\mu\text{m}$ , and two Al–O features around 12.59  $\mu\text{m}$  and 13.29  $\mu\text{m}$ ; absorption bands near 10.66  $\mu\text{m}$  and 10.94  $\mu\text{m}$  correspond to inner Al–OH bonds; the outer OH groups present features at lower wavelengths between 2.70  $\mu\text{m}$  and 2.77  $\mu\text{m}$ . Presence of

bonded molecular water, not from the kaolinite structure but due to atmospheric exposure, has absorption band near 2.78  $\mu\text{m}$  and 6.13  $\mu\text{m}$  (Johnston 2017). In the SWIR range, the first overtone of the OH vibration is present at 1.41  $\mu\text{m}$ , the combination tones of the OH and Al–OH generates a double absorption band at 2.16  $\mu\text{m}$  and 2.21  $\mu\text{m}$ , and the overtones of water are near 1.38  $\mu\text{m}$ , 1.45  $\mu\text{m}$ , and 1.88  $\mu\text{m}$ .

In the transformation toward metakaolinite, the main changes are related to the loss of OH groups. Miller (1961) described how in the dehydroxylation process, the bands near 2.77  $\mu\text{m}$  merge and the Al–OH bands at 10.66  $\mu\text{m}$  and 10.94  $\mu\text{m}$  vanishes indicating the destruction of the octahedral sheet. Percival et al. (1974) and Freund (1974) added that the Si–O bands merge and shift toward lower wavelengths, forming a broad absorption band around 9.35  $\mu\text{m}$  and a new band emerges near 12.39  $\mu\text{m}$  from the newly bonded Al–O.

### Metakaolinite–mullite transition

In the high-temperature domain (900–1200°C), metakaolinite re-crystallizes into a spinel phase. The reaction and the processes that undergo these transformations have been object of extensive research, and they are still subject of debate. According to Percival et al. (1974) and Gualtieri and Bellotto (1998), metakaolinite decomposes first into  $\gamma$ -alumina and Si-spinel, and later to mullite. The underwent chemical reactions are summarized by Ptáček et al. (2011) as follows:



The calcination reactions alter the surface properties of the clay mineral, as demonstrated by Drzal et al. (1983) and Bundy (1993), affecting the reactivity of the material. In particular, amorphous  $\gamma$ -alumina is highly reactive, and crystalline  $\gamma$ -alumina has a high water adsorption capacity, as

Maciver et al. (1963) and Peri (1965) verified. In the IR spectrum (Figure 1), the amorphous phases typically have broad absorption bands that shift toward lower wavelengths, near 8.33  $\mu\text{m}$  for the Si-spinel and toward 11.90  $\mu\text{m}$  for the  $\gamma$ -alumina. Well-developed Si–O absorption bands near 8.55  $\mu\text{m}$  and 11.10  $\mu\text{m}$  and Al–O absorptions near 13.51  $\mu\text{m}$  characterize the crystallization of mullite.

### 2.2 Infrared spectroscopy modes

Infrared reflectance spectroscopy uses the radiation that is reflected or scattered from a target material. Different modes of analyses are possible depending on the kind of reflection and the geometry of the instruments. King et al. (2004) summarized the methods commonly used for geological applications; among them, attenuated total reflectance (ATR), directional-hemispherical reflectance (DHR), and bidirectional reflectance were chosen for this study.

For laboratory characterization, ATR spectroscopy is perhaps the most used method. The ATR makes use of a special prism to produce internal reflections from the surface of a given material. By making full contact with the sample surface, it measures an evanescent wave generally recorded in the MWIR and LWIR ranges. DHR is mostly used to collect scattered energy integrating all reflection directions over a complete hemisphere. For acquiring this spectrum, an integrating sphere coated with a surface that is diffusely reflective to IR radiation is commonly used. The spectrum is typically recorded in the MWIR and LWIR ranges. However, its quality depends on the particle size of the samples (Salisbury and Wald 1992). Particularly, the DHR spectrum is affected by the transparency features in the long-wavelength region, as a consequence of the high volume scattering due to the small particle size (Cooper et al. 2002). Bidirectional reflectance, also known as external reflectance, uses an incident IR beam at an air/sample interface; the intensity of the reflected beam depends on the direction of the incident energy and the surface characteristics of the sample. The bidirectional reflectance

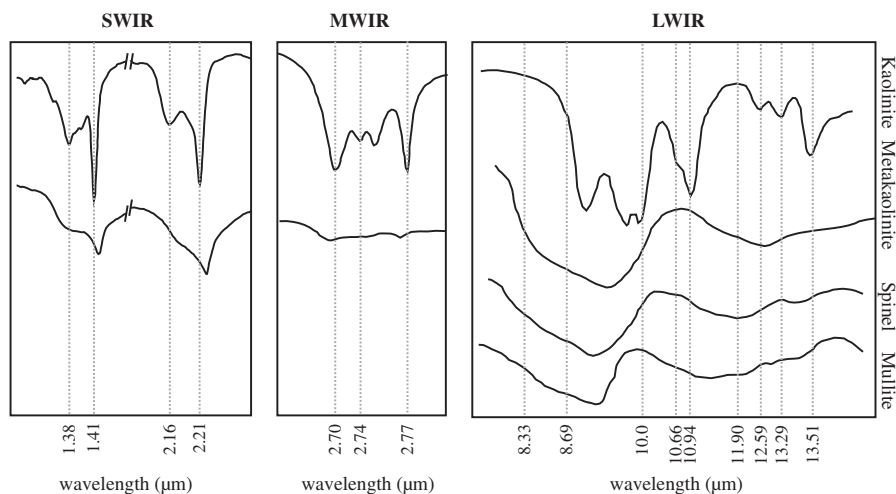


Figure 1. Main infrared spectral features that characterize the kaolin calcination process in the SWIR (Frost et al. 2002), MWIR (Drits et al. 2016), and LWIR (Percival et al. 1974) ranges.

mode is preferred in remote sensing, hand-held, and on-site applications the VNIR and SWIR ranges.

### 3 Methods

This study used three commercial kaolin samples thermally treated to 500°C from a kaolin processing plant in Cornwall (South-west England) (Wilson 2003). The kaolin in this area is well-known for its high purity and maturity due to the geological processes that led to its origin. The samples were taken from the production route after bleaching, demagnetizing, and milling, and they are representative of the typical feeds used for calcination. The samples were calcined in the laboratory using a muffle furnace attempting to emulate the conditions normally used in industrial operations where soak calcination is performed. Soak calcination involves exposing kaolin to high temperatures for a prolonged amount of time to guarantee complete calcination. Each sample was calcined at temperatures from 500°C to 1200°C at 100°C intervals. For each experiment, 360 gr of kaolin were equally split into six fused-silica dishes and placed in the calciner and heated from ambient to the specified temperature at a rate of 15°C per minute. The calciner was kept at the specified temperature for 15 min and then allowed to cool naturally. Once the temperature had cooled below 200°C, the sample was taken out and replaced with the next one. The samples were named *Ka-b*, with *a* being the sample number and *b* the calcination temperature. For this study, access was not granted to untreated samples; however, since the thermal behavior or partially dehydroxylated kaolin samples are qualitatively similar to that of untreated samples (Drits et al. 2016), the samples calcined at 500°C are regarded here as untreated kaolin. Table 2 shows the chemical composition of the reference kaolin determined with X-ray diffraction (XRF) data. According to semi-quantitative XRD analysis in combination with the bulk chemical analysis, the mineralogical content is approximately 65% kaolinite and 35% illite.

The XRD patterns were collected with a Bruker D8 Advance Diffractometer (Almelo, The Netherlands) featuring Bragg Brentano geometry using a Cu-K $\alpha$  radiation of 45 kV and 40 mA on powders placed on a PMMA holder L25. The XRD spectra were measured with a coupled  $\theta$ - $2\theta$  scan ranging from 10° to 110°  $2\theta$  (step size: 0.03°  $2\theta$ , time per step: 1 s). The acquired XRD patterns were interpreted by using the Bruker software DIFFRAC.EVA V4.2. A further interpretation was attempted with the Rietveld Software EXPGUI (Los Alamos, CA, USA).

Information on the thermal degradation of the reference kaolin samples was obtained by thermogravimetry analysis (TGA). The measurements were carried out with a Perkin Elmer TGA 8000

(Shelton, CT, USA). Samples of  $\pm 10$  were placed in an alumina pan and flushed with an N<sub>2</sub> carrier gas (30 ml/min). The samples were heated at 15°C per minute up to 1150°C, with an isothermal period of 15 min. The experiments were performed in replicates.

The kaolin calcination reaction was characterized with three spectroscopy methods. ATR was used for identifying the fundamental absorption bands of the samples. The measurements were collected on pressed powder using a Perkin Elmer Spectrum 100 FTIR spectrometer, using a diamond crystal. The data were originally recorded in wavenumbers and later transformed into micrometers. The spectral range covered from 4000 to 600 cm<sup>-1</sup> (2.5–16.67  $\mu$ m), the spectral resolution was 2 cm<sup>-1</sup>, and 16 scans were collected for every sample. The ATR spectrum tends to be weak at shorter wavelengths. Therefore, only the LWIR segment was used in the analysis. The DHR spectra were used to complement the ATR fundamentals data, ensuring good quality information in the MWIR. Besides, this technique was selected because the instrument set-up emulates the measuring conditions present in remote sensing applications. The measurements were collected on loosely packed powders using a Bruker Vertex 70 FTIR instrument adapted for DHR with an external integrating sphere. Details on the spectrometer design can be found in Hecker et al. (2011). Akin to ATR, DHR data were originally recorded in wavenumbers and later converted to micrometers. The spectra were collected in the 4000–625 cm<sup>-1</sup> range (2.50–16.00  $\mu$ m), at a resolution of 4 cm<sup>-1</sup> and 4096 scans per sample. Only the MWIR range was used in the analysis. Bidirectional reflectance was used as an intended on-site technique. The measurements were collected on compact powders with a rough surface, using an ASD field spectrometer with a contact probe and an internal light source. The spectra were collected in the visible, VNIR, and SWIR ranges, although only the SWIR range was used in the analyses; the spectral resolution was 0.01  $\mu$ m, and 50 scans were collected per sample.

Spectral data processing included removal of the continuum to normalize the reflectance spectra, thus enabling a better comparison of certain spectral features. The continuum, or background spectrum, is the overall albedo of the reflectance curve. It can be modeled as a mathematical function to isolate specific absorption bands, as it is explained by Clark and Roush (1984). The continuum was removed by using a built function in the Envi™ software (ITT, 2008) that calculates straight-line segments tangential to the spectra. The continuum removal (CR) was done independently for the 1.30–1.50, 1.80–2.10, 2.10–2.30, 5.50–6.50, and 7.50–15.00  $\mu$ m regions, and it was extracted for the spectral analysis of the sharpness of the LWIR Si–O and Al–O features, kaolinite crystallinity (Kx) index and 1900D parameter. Specific spectral values, such as reflectance and wavelength position were retrieved using the HypPy Hyperspectral Python Software Package developed by Bakker (2016). The general noise in the spectra was reduced using a Savitzky-Golay filter.

The sharpness of the Si–O absorption band around 9.50  $\mu$ m was determined by calculating the changes in the full-width half maximum (FWHM) constrained between 7.70  $\mu$ m and 10.90  $\mu$ m. The development of an Al–O absorption band around 13.70  $\mu$ m was determined using a slope

**Table 2.** Chemical composition (XRF) of the three kaolinite samples (wt.%).

Sample	Al <sub>2</sub> O <sub>3</sub>	SiO <sub>2</sub>	K <sub>2</sub> O	Fe <sub>2</sub> O <sub>3</sub>	TiO <sub>2</sub>	CaO	MgO	Na <sub>2</sub> O	P <sub>2</sub> O <sub>5</sub>	LOI(Lost
										On
										Ignition)
K1-500	37.0	48.0	1.45	0.65	0.03	0.08	0.31	0.06	0.11	12.3
K2-500	36.7	47.5	1.63	0.92	0.05	0.43	0.38	0.02	0.14	12.3
K3-500	37.2	47.0	1.15	1.43	0.04	0.06	0.26	0.01	0.16	12.6

parameter, named in this work as the 13.70 *slope*. It represents the slope between 13.30  $\mu\text{m}$  and 13.75  $\mu\text{m}$  and it was calculated as the ratio of the reflectance value at 13.30  $\mu\text{m}$  over that at 13.75  $\mu\text{m}$ . The slope between these values denotes the intensity of the 13.70  $\mu\text{m}$  absorption band.

The extraction of the Kx index was based on the parameters defined by Pontual et al. (1997). This index makes use of the characteristic doublet of kaolinite around 2.20  $\mu\text{m}$  to assess its degree of crystallinity. The determination of the Kx index is based on the formula:

$$\text{Kx} = (R_{2.184}/R_{2.190}) - ((R_{2.164}/R_{2.177}) - (R_{2.184}/R_{2.190})) \quad (4)$$

where  $R_x$  is the reflectance value at the given  $x$  wavelength, extracted from continuum removed spectra (Figure 2a). Well-defined doublets with steep slopes produce  $\text{Kx} \geq 1$ , characteristic of highly crystalline kaolinites, whereas for smooth doublets  $\text{Kx} < 1$  defining those that are poorly crystalline.

The 1900D parameter in this work is defined as the relative absorption depth of the minimum point in the 1.86–2.06  $\mu\text{m}$  region. The parameter was calculated on continuum removed spectra according to the definition of van der Meer (2004) as:

$$D = 1 - (R_b/R_c) \quad (5)$$

where  $\geq 1$  is the reflectance at the bottom of the absorption band and  $\geq 1$  is the reflectance of the continuum at the same wavelength as  $\geq 1$ , as represented in Figure 2b. The S1 and S2 points represent the shoulders that constrain the width of the absorption band at 1.86  $\mu\text{m}$  and 2.06  $\mu\text{m}$ , respectively. The 1900D parameter represents the intensity of the water absorption feature.

Soluble  $\text{Al}_2\text{O}_3$  was used as reference data to estimate the extent of the calcination reaction. It was chosen since it is the standard method utilized for quality control in some of the kaolin processing plants, such as the operations in Cornwall. This parameter measures the amount of  $\text{Al}_2\text{O}_3$  extracted from the  $\gamma$ -alumina in the spinel phase and, therefore, it is an indication of the stability of the minerals crystal structure. The soluble  $\text{Al}_2\text{O}_3$  was extracted by leaching using nitric acid following the procedure presented by Thomas (2010). The  $\text{Al}_2\text{O}_3$  content was measured using XRF analysis and is reported in Table 3.

The amount of environmentally adsorbed water (Table 3) was assessed by drying the samples overnight in an oven at 105°C and later exposing them to ambient conditions. The weight increase between the dry and exposed samples is taken as the relative amount of adsorbed water. This procedure was followed to ensure that the environmental conditions and time of exposure would be equal for all the samples.

## 4 Results and discussion

### 4.1 Characterization of calcined kaolin

The XRD patterns of the calcined kaolin samples, summarized in Figure 3, enabled the identification of the mineralogical content along the calcination stages. In the low temperatures (500–800°C), kaolinite is identified by the diffraction peaks at 25°  $2\theta$  ( $d(002) = 0.36$  nm), 20°  $2\theta$  ( $d(020) = 0.44$  nm), and 12°  $2\theta$  ( $d(001) = 0.71$  nm); in the reference kaolin, approximately 65% consists of kaolinite. The diffraction peaks around 9°, 18° and 27°  $2\theta$  are assigned to illite based on the chemical composition of the samples. From 500°C to 800°C, the reducing intensity of the kaolinite's diffraction peaks indicates breakdown of the crystal structure. Besides, increasing lump from 15° to 35°  $2\theta$  indicates the formation of an amorphous phase, attributed to metakaolinite. The presence of other diffraction peaks indicates the occurrence of crystalline phases attributed to illite and quartz, which remain present along the entire calcination sequence in an amount that varied from 35% to 45% for illite and from 10% to 15% for quartz. After 900°C, the diffraction peaks of kaolinite are completely absent, indicating complete dehydroxylation. At 1100°C, the development of new crystalline phases becomes evident by the emerging diffraction peaks characteristic of  $\gamma$ -alumina (37°, 46° and 67°  $2\theta$ ) and mullite (16°, 33°, 41°, 61° and 74°  $2\theta$ ), following the reaction presented in Equations (2) and (3) although possibly amorphous  $\gamma$ -alumina already occurs at slightly lower temperatures, namely around 1000°C.

In order to characterize the thermal transformations of the studied samples, TGA and Differential Thermal Analysis (DTA) analyses were conducted for the reference kaolin, as Figure 4 shows. Since the reference kaolin has been already

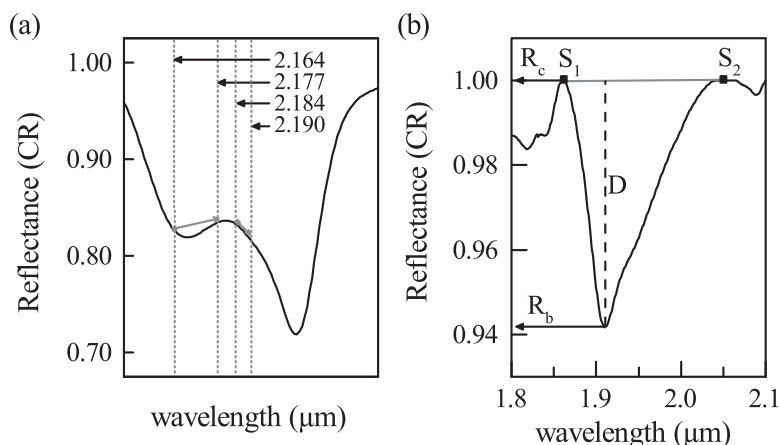
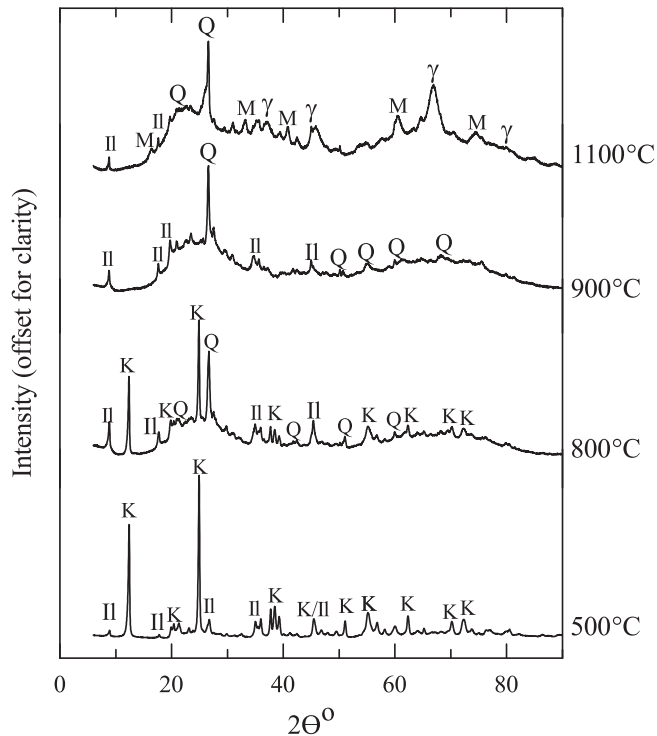


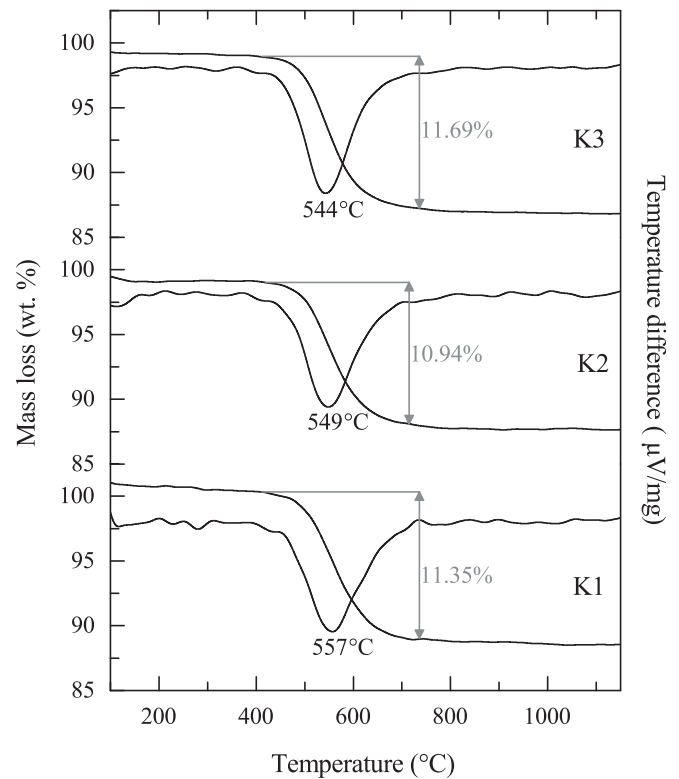
Figure 2. Definition of the spectral feature characteristics used in the extraction of the: (a) Kx index and (b) 1900D parameter (spectra were taken from sample K1-500).

**Table 3.** Soluble Al<sub>2</sub>O<sub>3</sub> values and mass increase due to environmentally adsorbed water of the calcined sample.

Sample	Soluble Al <sub>2</sub> O <sub>3</sub> (wt.%)	Mass increase (wt.%)
K1-500	0.51	0.41
K1-600	2.99	0.32
K1-700	13.3	0.42
K1-800	19.7	0.31
K1-900	23.5	0.21
K1-1000	18.8	0.29
K1-1100	10.2	0.31
K1-1200	1.58	0.46
K2-500	0.45	0.39
K2-600	3.51	0.45
K2-700	15.3	0.39
K2-800	16.3	0.32
K2-900	20.6	0.20
K2-1000	18.3	0.10
K2-1100	9.92	0.28
K2-1200	3.24	0.36
K3-500	0.54	0.36
K3-600	3.28	0.40
K3-700	9.52	0.40
K3-800	15.5	0.20
K3-900	21.6	0.11
K3-1000	21.0	0.30
K3-1100	8.15	0.38
K3-1200	1.25	0.42

**Figure 3.** XRD patterns of calcined kaolin at 500°C, 800°C, 900°C, and 1100°C where the most relevant mineralogical changes are detected. K = kaolinite, II = illite, Q = quartz,  $\gamma$  =  $\gamma$ -alumina, M = mullite (patterns are from K1 samples).

calcined to 500°C, the mass loss related to dehydration and pre-dehydroxylation is lower than that of natural kaolins. However, according to Drits et al. (2016), the patterns along the rest of the heating sequence are qualitatively similar. The dehydroxylation of kaolinite occurs from 420°C to 730°C, with the endothermic peak around 550°C, characteristic of high-crystallinity kaolinites. The exothermic peak that indicates the formation of  $\gamma$ -alumina around 985°C is weak suggesting mild recrystallization, probably due to the heating rate

**Figure 4.** TGA and DTA curves of kaolin partially dehydroxylated to 500°C.

and good crystallinity of the kaolinite. The asymmetry of the 550°C endothermic peak indicates the presence of illite, as previously indicated by the XRD analysis.

#### 4.2 Kaolin calcination reaction in the MWIR and LWIR ranges

The MWIR and LWIR measured spectra of the kaolin calcination are displayed in Figure 5. The spectra are divided into three regions to highlight the main absorption bands that characterize the reaction sequence. The first region (2.60–3.00  $\mu\text{m}$ ) shows the variation in the outer hydroxyls (Figure 5a); the second region (5.5–6.50  $\mu\text{m}$ ) displays the spectral absorption bands of molecular water (Figure 5b); the third one (8.00–14.00  $\mu\text{m}$ ) shows the aluminosilicate and the Al-hydroxyl absorption bands (Figure 5c and d). The most notorious change in the overall spectra occurs between 800°C and 900°C with a considerable reduction in the number of troughs, resulting in a transformation in the shape of the absorption bands.

The spectral changes in the low-temperature domain (500–800°C) clearly describe the dehydroxylation process that occurs in the kaolinite–metakaolinite transition. Most of the spectral absorption bands weaken as a result of the gradual breakdown of the kaolinite structure. The biggest changes occur in the MWIR range, where multiple bands between 2.70  $\mu\text{m}$  and 2.77  $\mu\text{m}$  become gradually shallower and suddenly fuse to a single and broad absorption band between 800°C and 900°C, reflecting the loss of OH groups. Similarly, the Si–O absorption bands in the LWIR range merge into a single band with minimum at 9.66  $\mu\text{m}$ , indicating the

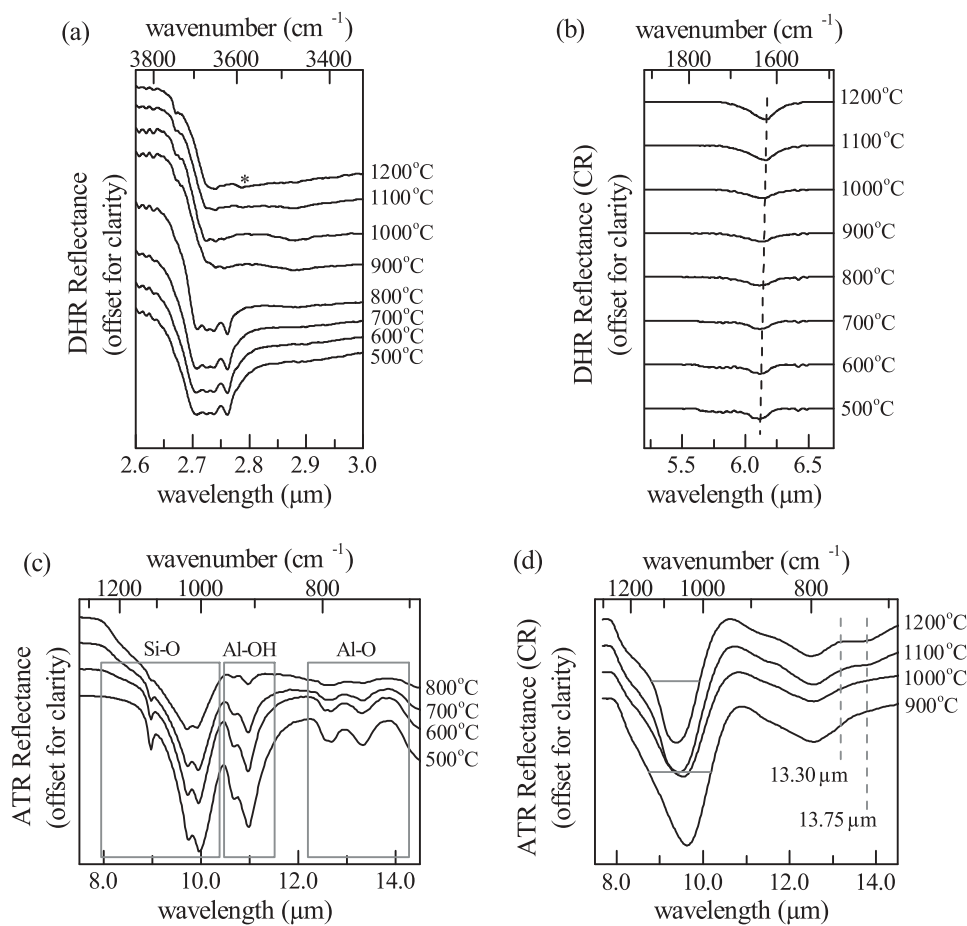


**Figure 5.** Infrared spectra of the calcined kaolin (sample K1). (a) Outer hydroxyls in the MWIR range at 2.63–3.13  $\mu\text{m}$  in DHR reflectance (the \* symbol indicates the trough at 2.78  $\mu\text{m}$ ); (b) diagnostic water absorption band in the MWIR range at 5.63–6.77  $\mu\text{m}$  in CR DHR reflectance; (c) aluminosilicate and Al-hydroxyl absorption bands in the LWIR range at 7.50–14.50  $\mu\text{m}$  in ATR reflectance between 500°C and 800°C; (d) enhanced CR ATR spectra between 900°C and 1200°C; horizontal bars in the Si–O band denote differences in the FWHM, and vertical dashed lines indicate the wavelengths used in the 13.70 slope for the Al–O feature.

transition toward an amorphous phase. The Al–O and water absorption bands become shallower, nearly flat, with the increasing temperature as a consequence of the water loss described in Equation (1). Furthermore, the complete fading of the Al–OH absorption band between 800°C and 900°C indicates that the dehydroxylation is complete, giving place to the metakaolinite phase.

In the high-temperature domain, from 900°C to 1200°C, broad and smooth bands that are particular of amorphous phases prevail. In the MWIR range, a weak hydroxyl band is constant at 2.74  $\mu\text{m}$ , as indication of the presence of illite previously identified with XRD. Besides, a new weak trough develops at 2.78  $\mu\text{m}$ , which is attributed by Aines and Rossman (1984) to the presence of molecular water; in addition, the deepening of the characteristic water absorption band at 6.13  $\mu\text{m}$  at higher temperatures (Figure 5b) reinforces this interpretation. The most prominent bands appear in the LWIR range (Figure 5d) where the Si–O single absorption band is dominant. This feature shifts to shorter wavelengths, and it constantly narrows toward the highest temperature, as the decrease in the FWHM values indicates (Figure 6a); besides, a shoulder appears at 9.09  $\mu\text{m}$  in the 1200°C spectrum. Even though the presence of illite (9.2  $\mu\text{m}$ ) and quartz (9.7  $\mu\text{m}$ ) in the high-temperature domain should be reflected

in the Si–O feature, it seems that the amorphous fraction masks these absorptions. The Al–O feature keeps a weak band around 12.63  $\mu\text{m}$ , which becomes mildly better defined at 1100°C and 1200°C. After 1100°C, the emergence of a new absorption band at 13.76  $\mu\text{m}$  is denoted by the 13.70 slope parameter, shown in Figure 6b, which indicates the continuous increasing intensity around this wavelength.

The redefinition of the Si–O and Al–O absorption bands at the highest temperatures suggest the beginning of the re-crystallization of the spinel phase, described in Equation (3). These results are consistent with data obtained by Percival et al. (1974), who described the spinel as Si-spinel and  $\gamma$ -alumina. However, in Figure 5d, the band centers for the Si–O and Al–O features are located at longer wavelengths than those reported in the literature (Section 2.1), indicating in the studied samples that the amorphous phase is dominant, which is in agreement with the TGA results that suggested that only mild recrystallization takes place. For the given experimental design, the temperature range where the metakaolinite and spinel phase are developed is also consistent with the time-temperature-transformation diagrams for kaolinite presented by Onike et al. (1986).

Maciver et al. (1963) indicated that  $\gamma$ -alumina strongly adsorbs molecular water on its surface. Moreover, Liu (2008) attributes the presence of a broad 2.84  $\mu\text{m}$  absorption band to

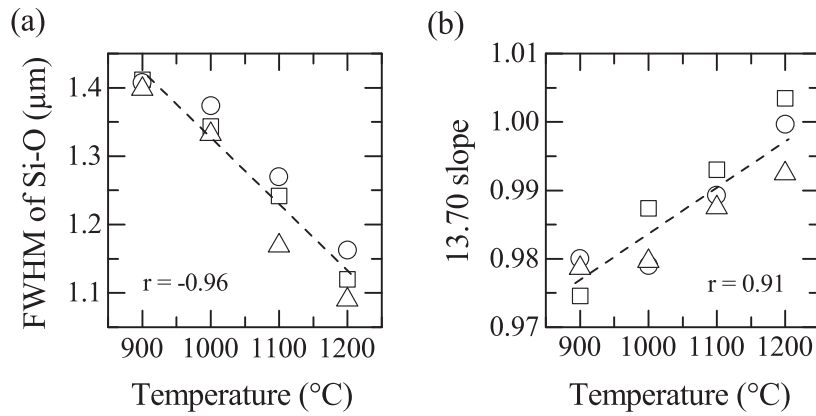


**Figure 6.** Spectral parameters that describe the redefinition of the Si-O and Al-O features in the high-temperature domain: (a) FWHM of the Si-O feature around 9.50 μm and (b) 13.70 slope parameter that indicates the formation of the Al-O absorption band (□ = K1, ○ = K2, △ = K3).

adsorbed water in hydrated  $\gamma$ -alumina. Since the studied samples were exposed to environmental conditions, it is expected that the presence of the  $\gamma$ -alumina phase formed from the metakaolinite is responsible for the re-adsorption of water once the sample has cooled down, and consequently, for the changes in the 2.78 μm and 6.13 μm absorption bands in the high-temperature domain. Therefore, the changes in the water absorption band are attributed to environmental conditions and not to the actual mineral transition. Most of the studies that characterize the metakaolinite–mullite transition focus on the description of the aluminosilicate bands. However, the evidence presented here supports the use of water-related absorption bands for the identification of  $\gamma$ -alumina, in conditions where the samples are exposed to the environment.

### 4.3 Kaolin calcination reaction in the SWIR range

The overtones and combination of the hydroxyl bands in the SWIR reflectance spectra are presented in Figure 7. In this

range, the doublets at 1.41 μm and 2.21 μm are diagnostic for the identification of kaolinite. In the low-temperature domain, these doublets gradually smoothen with the temperature rise, illustrating the extent of the dehydroxylation reaction and the transition toward the metakaolinite phase. Based on the 2.21 μm double absorption band, the Kaolinite crystallinity (Kx) index has been commonly used to characterize different types of kaolinite. Since this band is a combination of all the hydroxyl-related fundamentals, it might also give a good representation of the kaolinite dehydroxylation process. The Kx index makes use of the sharpness of the 2.21 μm doublet as a measure of the structural ordering in the kaolinite. Since the kaolinite–metakaolinite transition involves precisely a change in the crystal structure, the Kx index seems adequate to characterize these processes.

In Figure 8, the Kx index is used to characterize the kaolinite–metakaolinite transition. The Kx vs temperature plot (Figure 8a) shows the changes in crystallinity in relation to the temperature. According to the classification of Pontual et al. (1997), the kaolinite at 500°C is a very highly crystalline

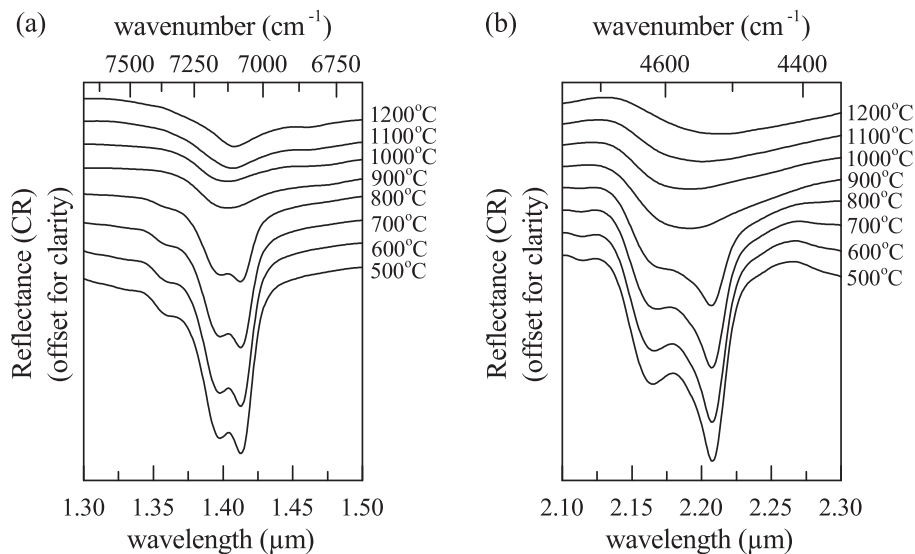


**Figure 7.** Hydroxyl overtones and combinations in the SWIR bidirectional reflectance spectra of the calcined kaolin (sample K1): (a) 1.30–1.50 μm and (b) 2.10–2.30 μm range.



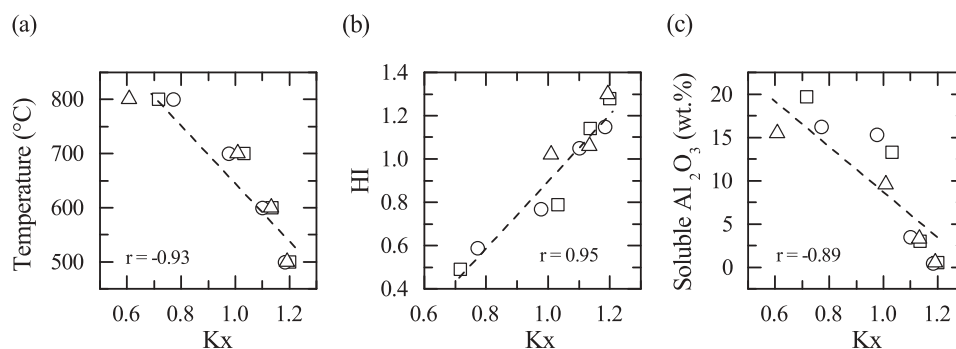


**Figure 8.** Relationship of the SWIR Kx index with (a) temperature, (b) Hinckley index (HI), and (c) soluble  $\text{Al}_2\text{O}_3$  (right)  $\square = \text{K1}$ ,  $\circ = \text{K2}$ ,  $\triangle = \text{K3}$ ; error bars are smaller than plot symbols).

kaolinite, at 700°C has degraded to a poorly crystalline kaolinite, and at 800°C is a very poorly crystalline kaolinite. The scatter plot reveals that dehydroxylation is rather a linear process, even though between 700°C and 800°C there is a sudden decrease of the Kx index. According to the XRD data, at 800°C the proportion of illite ( $\geq 1$ ) is higher than that of kaolinite ( $\geq 1$ ). Illite presents a single sharp absorption band at 2.21  $\mu\text{m}$  that smoothens the kaolinite doublet and decreases the Kx index values. Consequently, the crystallinity of kaolinite at this point should be slightly higher than indicated by the index. The XRD Hinckley Index (HI), which is commonly taken as the standard test in the analysis of the crystal structure of kaolinite (Plancon et al. 1988), was used to assess the influence of illite on the kaolinite analysis. The Pearson product moment correlation coefficient computed between the Kx and HI indices, displayed in Figure 8b, shows a strong positive correlation ( $\geq 1$ ), thus indicating that the presence of illite does not substantially influence the Kx values. In this way, the use of the Kx could probably offer a quantitative analysis of the dehydroxylation process.

In order to assess the suitability of the Kx index as a parameter to monitor the calcination reaction, a Pearson product-moment correlation coefficient was computed again to determine the relationship between the Kx values and the industrial standard, which is soluble  $\text{Al}_2\text{O}_3$ . The scatterplot in Figure 8c shows how, in the low-temperature domain, the amount of soluble  $\text{Al}_2\text{O}_3$  increases with the temperature, as previously shown in Table 3. Consequently, the Kx vs soluble  $\text{Al}_2\text{O}_3$  plot illustrates a negative yet nearly linear correlation between these parameters. For the very highly crystalline kaolinite ( $\geq 1$ ), the release of soluble  $\text{Al}_2\text{O}_3$  is very low, given that the crystal structure is still very stable. In the poorly ( $\geq 1$ ) and very poorly ( $\geq 1$ ) crystalline kaolinite, the soluble  $\text{Al}_2\text{O}_3$  strongly increases, since the crystal lattice weakens, and the kaolinite becomes more susceptible to chemical attack. However, the precise aluminum values vary among the three samples. This variation can be due to impurities in the chemical composition of the primary kaolinite, which might have greater influence on the structural stability at higher temperatures. Nevertheless, a Pearson's  $r$  value of  $-0.89$  indicates that there is a good correspondence between kaolinite crystallinity and soluble  $\text{Al}_2\text{O}_3$ . The soluble  $\text{Al}_2\text{O}_3$  measurements for this study have an accuracy of 0.1%, although routine industrial checks lower the accuracy to 0.5%. These data must be

interpreted with caution since with the limited amount of samples it is not possible to estimate how accurate would the Kx index be as a proxy for soluble  $\text{Al}_2\text{O}_3$ . Moreover, the typical cut-off values of soluble  $\text{Al}_2\text{O}_3$  are between 15% and 20%, where the correlation with the Kx index is less clear. However, these results serve as a conceptual approach for the further development of the Kx index as a proxy for the measurement of soluble  $\text{Al}_2\text{O}_3$  in the kaolin calcination reaction.

The variations in the SWIR water absorption feature are shown in Figure 9. This feature tends to disappear in the kaolinite–metakaolinite transition, identical to what was observed in the MWIR spectra. Between 900°C and 1200°C, the deepening of the 1.90  $\mu\text{m}$  feature is remarkable. Similarly, the 1.41  $\mu\text{m}$  absorption band in Figure 3 sharpens in the same temperature range, and a new trough emerges near 1.45  $\mu\text{m}$ . From the MWIR spectral characterization, the patterns of these absorption bands are attributed to the increasing presence of molecular water adsorbed to the  $\gamma$ -alumina phase. Given that the aluminosilicate fundamentals do not present secondary absorption bands in the SWIR range, the spectral detection of water in calcined kaolin samples could be used as a parameter to detect the presence of  $\gamma$ -alumina that has been generated in the recrystallization phase from metakaolinite to mullite. Therefore, the depth of the 1.90  $\mu\text{m}$  water absorption

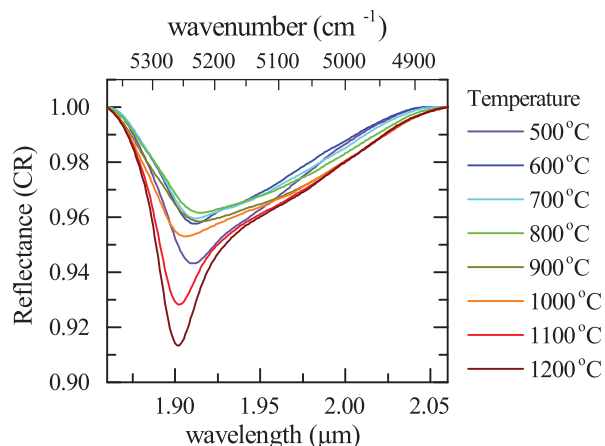


**Figure 9.** Changes in the depth of the water absorption feature (at 1.90  $\mu\text{m}$ ) in the SWIR bidirectional reflectance spectra of the calcined kaolin (sample K1).

band, defined as the 1900D parameter, seems to be convenient for the determination of the intermediate phases in the high-temperature domain.

Akin to the Kx index analysis, Pearson product-moment correlation coefficients were computed to assess the relationship between the 1900D parameter and the relevant variables in the high-temperature domain. First, in order to ensure that the 1.90  $\mu\text{m}$  absorption band is related to surface water, the correlation between the 1900D parameter and the adsorbed water measurement was assessed. Figure 10a shows that there is a positive correlation between these two variables, which indicates that the 1900D parameter is indeed related to water environmentally adsorbed in the materials surface. However, the coefficient value  $\geq 1$  suggests that the water absorption feature does not fully explain the amount of adsorbed water. The error of the adsorbed water measurements is 0.01%; therefore it does not significantly affect the analysis. The mismatch indicates that the amount of surface water is a more complex function that involves not only the exposition to the environment (i.e. time of exposure, humidity), but also the powder properties (i.e. particle size, packing density of the sample). All these variables would affect the 1900D parameter and therefore must be taken into account to improve its reliability as a proxy for the measurement of the soluble  $\text{Al}_2\text{O}_3$ , and for establishing the level of accuracy of the method. These topics should be a matter of further research.

The variation of the 1900D with the treatment temperature is presented in Figure 10b. The lowest 1900D values correspond to the metakaolinite phase between 900°C and 1000°C, and the depth increase is related to the transition from amorphous to crystalline  $\gamma$ -alumina, which corresponds to the process presented in Equations (2) and (3). The scatterplot shows that the deepening of the water absorption band has a strong positive correlation ( $\geq 1$ ) with the temperature increment. Figure 10c illustrates the relationship between the 1900D parameter and soluble  $\text{Al}_2\text{O}_3$ ; the correlation is negative yet strong ( $\geq 1$ ). Low 1900D values correspond to a high amount of soluble  $\text{Al}_2\text{O}_3$ , which fits well with the metakaolinite phase. With an increase in the water content, there is a drop in the soluble  $\text{Al}_2\text{O}_3$  values due to the gradual incorporation of alumina into the spinel phase. The good correlation between the 1900D parameter and the soluble  $\text{Al}_2\text{O}_3$  values indicates that the depth of the water absorption band measured in the SWIR spectra could be used as a proxy for the

amount of soluble  $\text{Al}_2\text{O}_3$ , and therefore, for the formation of  $\gamma$ -alumina. For a more accurate quantification of soluble  $\text{Al}_2\text{O}_3$  using the 1900D parameter, it would be needed to perform more refined statistical analysis.

#### 4.4 Implications for on-line characterization of the calcined kaolin reaction

Numerous researchers have studied the calcined kaolin reaction sequence. This continuous interest has been driven by the industrial importance of the products derived from the various calcination stages. Nevertheless, most of the published work focusses on the development of products with certain properties, rather than in the monitoring and control of the calcination process. For these applications, it is necessary to use techniques that can perform on-line measurements and provide information in real time. This study has taken advantage of the broad knowledge of the kaolin calcination process to make a step forward to the development of a monitoring and control strategy. More precisely, it has focused on the use of infrared spectroscopy in the MWIR and LWIR range to explore the feasibility of using the SWIR range as an alternative to estimate the extent of the calcination reaction in an on-line environment, offering a conceptual approach for the further development of this method.

The results of the MWIR and LWIR characterization agree with those of reference works, such as Frost (1998) and Percival et al. (1974). Furthermore, it also provides evidence of the presence of adsorbed water related to the  $\gamma$ -alumina phase, which can be used as a parameter for spectrally characterizing the high-temperature phases in the calcined kaolin sequence. The extrapolation of the MWIR and LWIR results to the SWIR range demonstrates that the kaolin calcination reaction can be entirely characterized by using SWIR spectroscopy. On the one hand, the kaolinite–metakaolinite transition is directly described by the variations in the 2.21  $\mu\text{m}$  band and can be quantified using the Kx index. On the other hand, the metakaolinite– $\gamma$ -alumina transition can be indirectly estimated by using the water absorption feature depth at 1.90  $\mu\text{m}$ . The good correlation of both, the Kx and the 1900D parameters with the soluble  $\text{Al}_2\text{O}_3$  values shows that these spectral parameters could be used as a proxy to quantify the extent of the kaolin calcination reaction.

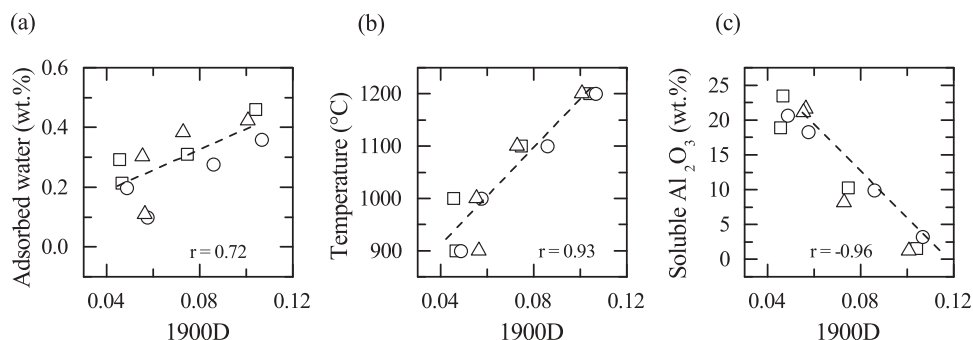


**Figure 10.** Variation in the depth of the 1.9  $\mu\text{m}$  absorption band (1900D parameter) compared with the changes in (a) adsorbed water, (b) temperature, and (c) soluble  $\text{Al}_2\text{O}_3$  ( $\square$  = K1,  $\circ$  = K2,  $\triangle$  = K3; error bars smaller are than plot symbols).

The present study raises the possibility of using SWIR spectroscopy as a technique for the monitoring and control of calcined kaolin process. The results presented in this work, offer the criteria needed to refine the Kx and 1900D parameters and transform them into a tool capable of quantifying the amount of soluble  $\text{Al}_2\text{O}_3$ . For this, specific Kx and 1900D thresholds that comply with the optimum soluble  $\text{Al}_2\text{O}_3$  values must be determined. Besides, the conditions for the implementation of an on-line analysis system should also be considered. In a kaolin processing plant, the calcination is performed in a Multiple Hearth Furnace, in which the temperature increases from hearth to hearth. The on-line spectral analysis would ideally be implemented by taking measurements of the feed for the calciner and at every hearth to track the evolution of the kaolin transformation sequence and establish the optimum point for the desired product.

## 5 Conclusions

This study has shown that the calcined kaolin reaction sequence can be entirely characterized using SWIR spectroscopy. The spectral changes are in good agreement with the XRD and TGA data, although quantitative analyses are required to verify the accuracy of the spectral characterization. Based on the results, the kaolinite crystallinity (Kx) index and the depth of the water absorption feature (1900D) were defined as spectral parameters that describe different steps in the calcination of kaolinite. The results were analyzed toward an assessment of the possibility of using SWIR spectroscopy as a technique for the on-line analysis of the calcination reaction.

The analysis of the MWIR and LWIR spectra of the calcined samples revealed the extent of the calcination reaction. In the first part of the reaction, the breakdown of the kaolinite structure is evidenced by the general weakening of the spectral absorption bands. Between 800°C and 900°C, the kaolinite dehydroxylation was complete giving place to the metakaolinite phase. The sharpening of the spectral absorption bands in the second part of the reaction indicated the formation of the spinel phase. The latter was accompanied by an increase in the intensity of the water spectral absorption band. This was attributed to physically absorbed water after exposure to the environment, which is a consequence of the  $\gamma$ -alumina presence. The spectral detection of adsorbed water accompanying the  $\gamma$ -alumina phase is one of the most significant findings that emerged from this study.

In the SWIR range, the changes in the 2.21  $\mu\text{m}$  band described the dehydroxylation of kaolinite; at this wavelength, the Kx index was used to measure the transition from kaolinite toward the amorphous metakaolinite, by showing the gradual loss of hydroxyl groups. The metakaolinite–spinel transition was indirectly interpreted from the 1900D parameter, which measures the increase in the water content, previously related to the formation of  $\gamma$ -alumina with the help of MWIR spectra.

The relevance of the utilization of the Kx index and 1900D parameter in the characterization of the calcined kaolin reaction is supported by their good correlation with the industry standard soluble  $\text{Al}_2\text{O}_3$  measurements. The results indicate

that the SWIR spectrum could be used to estimate the extent of the calcination reaction. In this sense, this research ultimately provides a framework for the development of an on-line analysis system based on SWIR spectroscopy, which ultimately would increase the consistency and quality of the calcined kaolin products. Such system would drastically reduce the turn-around time required for quality control, by minimizing the use of off-line measurements. Moreover, the type of samples and instruments support the practicality of using the proposed approach. Last but not least, the technology readiness would foster the tailoring and implementation of the technique in the kaolin production environment.

## Acknowledgments

The authors wish to thank Imerys Ltd., UK, for the access to the samples and the Faculty of Geo-Information Science and Earth Observation (ITC) of the University of Twente for the access to the Spectroscopy and Geosciences Laboratories. Ruud Hendrix at the Department of Materials Science and Engineering of the Delft University of Technology is acknowledged for the X-ray analysis.

## Disclosure statement

The authors report no conflicts of interest. The authors alone are responsible for the content and writing of the article.

## Funding

This work has been financially supported by the European FP7 project Sustainable Technologies for Calcined Industrial Minerals in Europe (STOICISM) [grant no. NMP2-LA-2012-310645].

## ORCID

A. Guatame-García  <http://orcid.org/0000-0002-9117-6655>

C. Hecker  <http://orcid.org/0000-0001-6802-5042>

## References

- Aines, R. D., and Rossman, G. R., 1984, "Water in minerals? A peak in the infrared." *Journal of Geophysical Research*, 89. pp. 4059–4071. Doi:10.1029/JB089iB06p04059.
- Bakker, W. HypPy hyperspectral python software package, 2016. URL <https://www.itc.nl/personal/bakker/hypy.html>.
- Brindley, G. W., and Nakahira, M., 1959a, "The kaolinite-mullite reaction series: I. A survey of outstanding problems." *Journal of the American Ceramic Society*, 42. pp. 311–314. Doi:10.1111/j.1151-2916.1959.tb14314.x.
- Brindley, G. W., and Nakahira, M., 1959b, "The kaolinite-mullite reaction series: II. Metakaolin." *Journal of the American Ceramic Society*, 42. pp. 314–318. Doi:10.1111/j.1151-2916.1959.tb14315.x.
- Brindley, G. W., and Nakahira, M., 1959c, "The kaolinite-mullite reaction series: III. The high-temperature phases." *Journal of the American Ceramic Society*, 42. pp. 319–324. Doi:10.1111/j.1151-2916.1959.tb14316.x.
- Bundy, W. M., 1993, The diverse industrial applications of kaolin, In *Kaolin Genesis and Utilisation: Keller '90 Kaolin Symposium, the Clay Minerals Society Special Publication*, (H. H. Murray, H. Haydn, W. M. Bundy, and C. C. Harvey, Eds.), Boulder, CO: Clay Minerals Society, ISBN: 9781881208051.
- Clark, R. N., and Roush, T. L., 1984, "Reflectance spectroscopy: quantitative analysis techniques for remote sensing applications." *Journal of Geophysical Research*, 89. pp. 6329–6340. Doi:10.1029/JB089iB07p06329.

- Cooper, B. L., Salisbury, J. W., Killen, R. M., and Potter, A. E., 2002, "Midinfrared spectral features of rocks and their powders." *Journal of Geophysical Research E: Planets*, 107. pp. 1-1 – 1-19. Doi:10.1029/2000JE001462.
- Drits, V. A., and Derkowski, A., 2015, "Kinetic behavior of partially dehydroxylated kaolinite." *American Mineralogist*, 100. pp. 883–896. Doi:10.2138/am-2015-5083.
- Drits, V. A., Derkowski, A., Sakharov, B. A., and Zviagina, B. B., 2016, "Experimental evidence of the formation of intermediate phases during transition of kaolinite into metakaolinite." *American Mineralogist*, 101. pp. 2331–2346. Doi:10.2138/am-2016-5776.
- Drzal, L. T., Rynd, J. P., and Fort, T., Jr, 1983, "Effects of calcination on the surface properties of kaolinite." *Journal of Colloid and Interface Science*, 93. pp. 126–139. Doi:10.1016/0021-9797(83)90392-2.
- Freund, F., 1974, *Ceramics and Thermal Transformation of Minerals, Volume Monograph 4, Book Section 20*, London: Mineralogical Society. pp. 465–482.
- Frost, R. L., 1998, "Hydroxyl deformation in kaolins." *Clays and Clay Minerals*, 46. pp. 280–289. Doi:10.1346/ccmn.1998.0460307.
- Frost, R. L., Mak, Kristf, J., and Kloprogge, J. T., 2002, "Modification of kaolinite surfaces through mechanochemical treatment – a mid-IR and near-IR spectroscopic study." *Spectrochimica Acta – Part A: Molecular and Biomolecular Spectroscopy*, 58. pp. 2849–2859. Doi:10.1016/S1386-1425(02)00033-1.
- Frost, R. L., and Vassallo, A. M., 1996, "The dehydroxylation of the kaolinite clay minerals using infrared emission spectroscopy." *Clays and Clay Minerals*, 44. pp. 635–651. Doi:10.1346/CCMN.1996.0440506.
- Gualtieri, A., and Bellotto, M., 1998, "Modelling the structure of the metastable phases in the reaction sequence kaolinite-mullite by X-ray scattering experiments." *Physics and Chemistry of Minerals*, 25. pp. 442–452. Doi:10.1007/s002690050134.
- Gupta, R.P. 2003, *Remote Sensing Geology, Berlin*: Springer-Verlag.
- Haavisto, O., and Hytyniemi, H., 2011, "Reflectance spectroscopy in the analysis of mineral flotation slurries." *Journal of Process Control*, 21. pp. 246–253. Doi:10.1016/j.jprocont.2010.10.015.
- Hackwell, J. A., et al. 1996, LWIR/MWIR imaging hyperspectral sensor for airborne and ground-based remote sensing. Proceedings SPIE 2819, Imaging Spectrometry II, Denver, CO, USA.
- Hecker, C., Hook, S., van der Meijde, M., Bakker, W., van Werff, H., Wilbrink, H., van Ruitenbeek, F., de Smeth, B., and van der Meer, F., 2011, "Thermal infrared spectrometer for earth science remote sensing applications-instrument modifications and measurement procedures." *Sensors*, 11. pp. 10981–10999. Doi:10.3390/s111110981.
- Heller-Kallai, L., 2013, Chapter 10.2 – Thermally modified clay minerals. In *Handbook of Clay Science, Volume 5 of Developments in Clay Science*, (F. Bergaya and G. Lagaly, Eds.), Amsterdam, The Netherlands: Elsevier, pp. 411–433. Doi:10.1016/B978-0-08-098258-8.00014-6.
- Johnston, C. T., 2017, Infrared studies of clay mineral-water interactions, In *Developments in Clay Science*, (W.P. Gates, J.T. Kloprogge, J. Madejová, F. Bergaya, Eds.), Amsterdam, The Netherlands: Elsevier, pp. 288–309. Doi:10.1016/b978-0-08-100355-8.00009-6.
- King, P. L., Ramsey, M. S., McMillan, P. F., and Swayze, G. A., 2004, *Laboratory Fourier Transform Infrared Spectroscopy Methods for Geologic Samples, Volume 33 of Short Course Series, Book Section* 3, Ottawa, Canada: Mineralogical Association of Canada, p. 36. ISBN: 9780921294337.
- Liu, X., 2008, "Drifts study of surface of  $\gamma$ -alumina and its dehydroxylation." *Journal of Physical Chemistry C*, 112. pp. 5066–5073. Doi:10.1021/jp711901s.
- Maciver, D. S., Tobin, H. H., and Barth, R. T., 1963, "Catalytic aluminas. I. Surface chemistry of eta and gamma alumina." *Journal of Catalysis*, 2. pp. 485–497. Doi:10.1016/0021-9517(63)90004-6.
- Miller, J. G., 1961, "An infrared spectroscopic study of the isothermal dehydroxylation of kaolinite at 470." *The Journal of Physical Chemistry*, 65. pp. 800–804. Doi:10.1021/j100823a023.
- Murray, H. H., and Lyons, S. C., 1959, Further correlations of kaolinite crystallinity with chemical and physical properties, In *Eighth National Conference on Clays and Clay Minerals, Clays and Clay Minerals*, (A. Swineford, Ed.), Norman, OK: Elsevier Science, Doi:10.1346/CCMN.1959.0080104.
- Onike, F., Martin, G. D., and Dunham, A. C., 1986, "Time-temperature-transformation curves for kaolinite." *Kinetics and Mass Transport in Silicate and Oxide Systems*. pp. 73–82. Doi:10.4028/www.scientific.net/MSF.7.73.
- Percival, H. J., Duncan, J. F., and Foster, P. K., 1974, "Interpretation of the kaolinite-mullite reaction sequence from infrared absorption spectra." *Journal of the American Ceramic Society*, 57. pp. 57–61. Doi:10.1111/j.1151-2916.1974.tb10813.x.
- Peri, J. B., 1965, "Infrared and gravimetric study of the surface hydration of  $\gamma$ -alumina." *Journal of Physical Chemistry*, 69. pp. 211–219. Doi:10.1021/j100885a032.
- Plancon, A., Giese, R. F., and Snyder, R., 1988, "The Hinckley index for kaolinites." *Clay Minerals*, 23. pp. 249–260. Doi:10.1180/claymin.1988.023.3.02.
- Pontual, S., Merry, N., and Gamson, P., 1997, *Regolith Logging, Volume 1, Book Section 8*, Perth, Australia: AusSpec International.
- Ptáček, P., Šoukal, F., Opravil, T., Nosková, M., Havlica, J., and Brandtšter, J., 2011, "Mid-infrared spectroscopic study of crystallization of cubic spinel phase from metakaolin." *Journal of Solid State Chemistry*, 184. 10. pp. 2661–2667. Doi:10.1016/j.jssc.2011.07.038.
- Salisbury, J. W., and Wald, A., 1992, "The role of volume scattering in reducing spectral contrast of reststrahlen bands in spectra of powdered minerals." *Icarus*, 96:0. pp. 121–128. Doi:10.1016/0019-1035(92)90009-V.
- Thomas, R., Grose, D., Obaje, G., Taylor, R., Rowson, N., and Blackburn, S., 2009, "Residence time investigation of a multiple hearth kiln using mineral tracers." *Chemical Engineering and Processing: Process Intensification*, 480. 4. pp. 950–954. Doi:10.1016/j.cep.2009.01.003.
- Thomas, R. E. *High temperature processing of kaolinitic materials*. University of Birmingham, 2010. URL <http://theses.bham.ac.uk/6075/>.
- van der Meer, F., 2004, "Analysis of spectral absorption features in hyperspectral imagery." *International Journal of Applied Earth Observation and Geoinformation*, 5 pp. 55–68. Doi:10.1016/j.jag.2003.09.001.
- Visual Information Solutions ITT 2008, *Envi*.
- Wilson, I. R., 2003, "Current World Status of Kaolin from South-West England." *Geoscience in South-West England*, 10. pp. 417–423. ISSN: 05663954.